[9] *JANAF Thermochemical Tables*, Dow Chemical Co., Midland, Mich.
[10] R. L. Wilkins, "Thermodynamics of SF_6 and its decomposition and oxidation products," Aerospace Rep. TR-0158 (32TO-20)-19; U. S. Air Force Rep. SAM-SD-TR-68-371, 1968.
[11] J. M. Yos, AVCO Tech. Mem. RAD-TM-63-7, ASTIA Doc. AD-435-053, 1963.
[12] R. S. Brokaw, "Thermal conductivity of gas mixtures in chemical equilibrium II," *J. Chem. Phys.*, vol. 32, April 1960.
[13] L. Spitzer, Jr., *Physics of Fully Ionized Gases*. New York: Interscience, 1956.
[14] B. W. Swanson and R. M. Roidt, "Boundary layer analysis of a SF_6 circuit breaker arc," *IEEE Trans. Power App. Syst.*, to be published. Our F is the same as their f_k.
——, "Some numerical solutions of the boundary layer equations for an SF_6 arc," this issue, pp. 493–501.
[15] V. R. Watson and E. B. Pegot, "Numerical calculations for the characteristics of a gas flowing axially through a constricted arc," NASA TN (1)-4042, June 1967.
[16] J. F. Perkins and L. S. Frost, "The behavior of gas blown SF_6 arcs in and insulating nozzle," *IEE Int. Conf. Gas Discharges* (London, Sept. 1970).
——, "The enthalpy flow limitation of gas-blasted SF_6 arcs," to be published.
[17] K. H. Yoon and H. E. Spindle, "A study of the dynamic response of arcs in various gases," *AIEE Trans. (Power App. Syst.)*, vol. 77, Feb. 1959, pp. 1634–1642.
[18] H. Motschmann, "Über die experimentelle Bestimmung der Wärmeleitfähigkeit und der elektrischen Leitfähigkeit von Wasserstoff und Schwefelhexafluorid im elektrischen Lichtbogen," *Z. Phys.*, vol. 191, 1966, pp. 10–23.
[19] D. J. Siddons and K. Heron, "High speed photographic study of the extinction of an SF_6 arc," *1969 Nottingham Univ. Power Engineering Conf.*, Paper 5.3.
[20] J. O. Hirschfelder, C. F. Curtiss, and R. B. Bird, *Molecular Theory of Gases and Liquids*. New York: Wiley, 1964.
[21] R. S. Brokaw, "Alignment charts for transport properties viscosity, thermal conductivity, and diffusion coefficients for nonpolar gases and gas mixtures," Lewis Res. Center, Cleveland, Ohio, NASA Tech. Rep. TR R-81, 1960.
[22] D. Rapp, and W. E. Francis, "Charge exchange between gaseous ions and atoms," *J. Chem. Phys.*, vol. 37, Dec. 1962, pp. 2631–2645.
[23] E. A. Mason and R. J. Munn, "Transport coefficients of ionized gases," *Phys. Fluids*, vol. 10, Aug. 1967, p. 1827.
[24] E. J. Robinson and S. Geltman, "Single- and double-quantum photodetachment of negative ions," *Phys. Rev.*, vol. 153, Jan. 1967, pp. 4–8.
[25] B. W. Swanson, see [14] and private communication.

Investigations of the Properties of SF_6 as an Arc Quenching Medium

WALTER HERTZ, HARALD MOTSCHMANN, AND HERMANN WITTEL

Abstract—The results of experiments on stationary and nonstationary arcs in SF_6 are summarized. High temperature gas properties, like the electrical and thermal conductivity as well as the theoretically predicted plasma demixing effects, are determined by electrical and spectroscopic measurements. Investigations on interrupted dc arcs give insight into the energy transport mechanism of the arcs. The transient temperature behavior of gas blast interrupted arcs is measured. Finally, the application of the investigations to circuit breaker arcs is discussed. The following principal results have been found: From the lower time constant of blown N_2 arcs in comparison to SF_6 arcs above 10 000 K it follows that the good quenching properties of SF_6 must be due to processes taking place below 10 000 K. This agrees also with the time-constant measurements in the interrupted cascade arc: at lower temperature—below approximately 8000 K—the conductance decay in N_2 is very much slower than in SF_6. Further, these measurements revealed that the steep descent in SF_6 is not caused by electron attachment but is due to energy transport mechanisms. Experimental work about the plasma properties on steady-state arcs, including demixing effects, is in good agreement with theory. Finally the ac experiments show that the temperature profile of the blown ac arcs has a nearly rectangular shape. Variations in current affect mainly the diameter of the arc whereas the temperature variations are fairly small.

Manuscript received September 28, 1970; revised December 17, 1970.
The authors are with the Siemens AG, Research Laboratory, Erlangen, Germany.

I. Introduction

POWER CIRCUIT breakers utilizing sulphur hexafluoride as the dielectric and quenching agent have now been in use for more than a decade and experience has shown that they exhibit excellent insulating and quenching properties [1]. The high dielectric strength is a result principally of the electronegative properties of the gas, i.e., of its readiness to form negative ions from neutral particles and electrons, but the mechanisms leading to efficient arc quenching using SF_6 are not yet fully understood.

At the present time, SF_6 circuit breakers capable of interrupting up to 50 kA at 110 kV and even more are available but continued research into the physics of the SF_6 arc is motivated by the demand for improvement in these voltage and current interruption specifications since in order to implement further improvement into existing designs a more complete understanding of the quenching processes is required.

The physical understanding of the quenching processes requires a knowledge of the SF_6 material data in the temper-

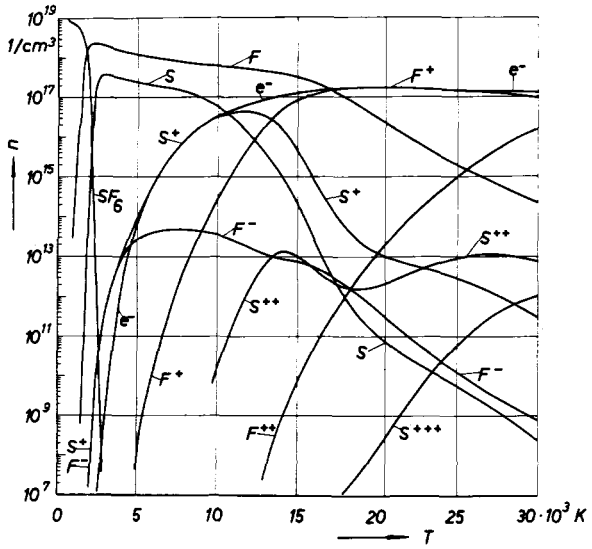

Fig. 1. Particle density diagram of SF_6.

ature range up to 30 000 K. Temperatures of this order can be reached on the axis of an arc.

In the following discussion, section II describes the results of computer calculations of particle densities carried out by Frie [2] and the material functions derived from them are presented and compared with available experimental data. In section III, electrical measurements on an interrupted dc arc without flow are described and the results are compared with those of time-resolved spectroscopic studies of the electrical conductance time constants. In the latter experiments the behavior of gases such as CO_2, N_2, and A was also studied for the purpose of comparison with the SF_6 data. A model of heat dissipation away from the inner arc regions for an arc with turbulent gas blast is also discussed. In conclusion, in section IV, measurements in which the experimental conditions were designed to simulate those found in actual circuit breakers are described. Such measurements lead to a further improvement in the understanding of the complicated arc processes occurring in these devices.

II. Measurement and Calculation of SF_6 Material Functions

Experimental determination of SF_6 material data as a function of temperature using an electric arc is complicated by the fact that because of the plasma conditions, direct spectroscopic methods of temperature measurement which are independent of the plasma composition cannot be applied. Consequently, calculation of the temperature dependence of the particle densities provides the basis for further theoretical and experimental studies of the required material properties.

The results of such calculations, obtained using the computer programme derived by Frie [2], for a pressure of 10^5 N/m^2 in the region up to 30 000 K are shown in Fig. 1. At moderate temperatures, 4000 K for example, the composition in the molecular region is highly complex. At 4000 K the molecules are almost completely dissociated while most of the electrons are still bound due to the formation of

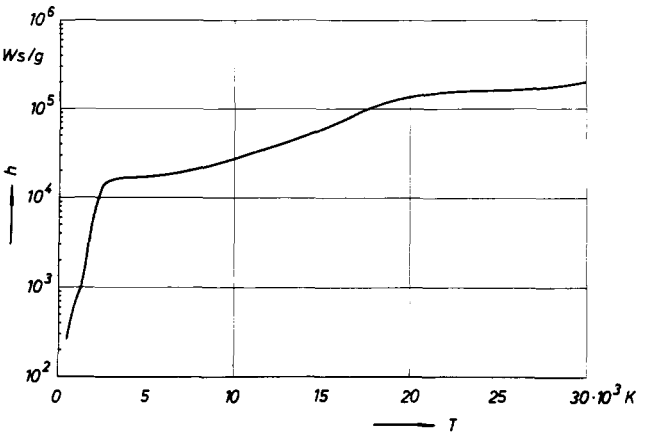

Fig. 2. Specific enthalpy $h(T)$ of SF_6.

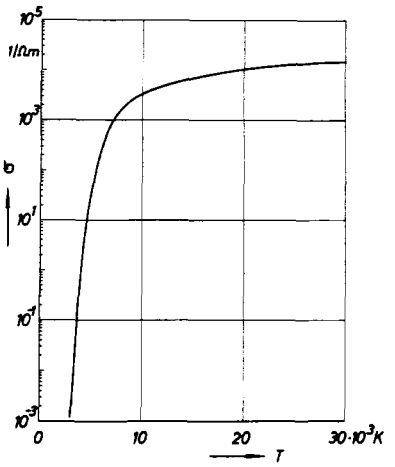

Fig. 3. Electrical conductivity $\sigma(T)$ of SF_6.

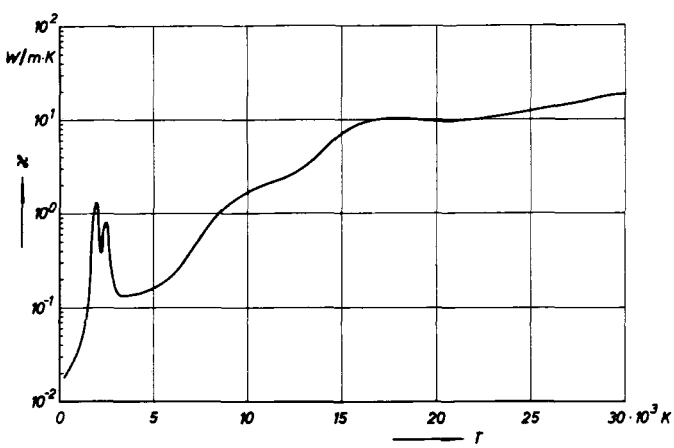

Fig. 4. Thermal conductivity $\kappa(T)$ of SF_6.

negative ions. The density of negative ions increases and remains between 10^{13} and 10^{14} cm^{-3} over a relatively wide temperature region ($\simeq$ 10 000 K). The diagram also shows the strong shift towards fluorine of the stoichiometric ratio of fluorine to sulphur at high temperatures, when demixing occurs. The computer calculations have also yielded the following material properties: density, specific enthalpy, specific heat, isentropic exponent, and velocity of sound as well as the electrical and thermal conductivity. The specific

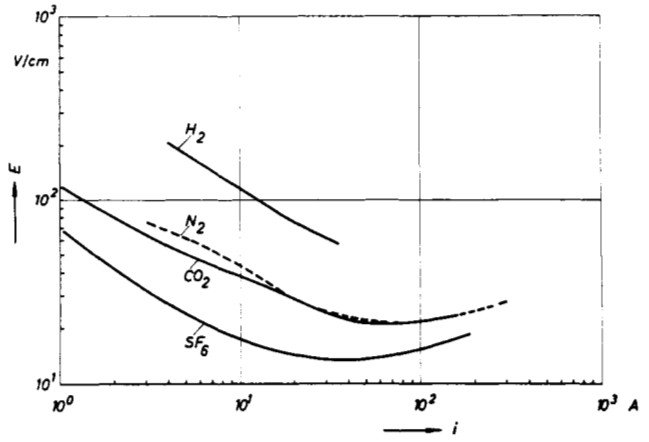

Fig. 5. Field-strength current characteristics $E(i)$.

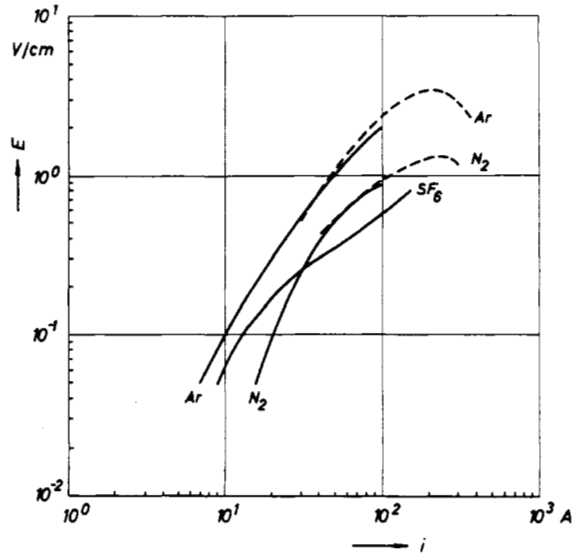

Fig. 6. Radiation characteristics in equivalent electrical field strengths versus current.

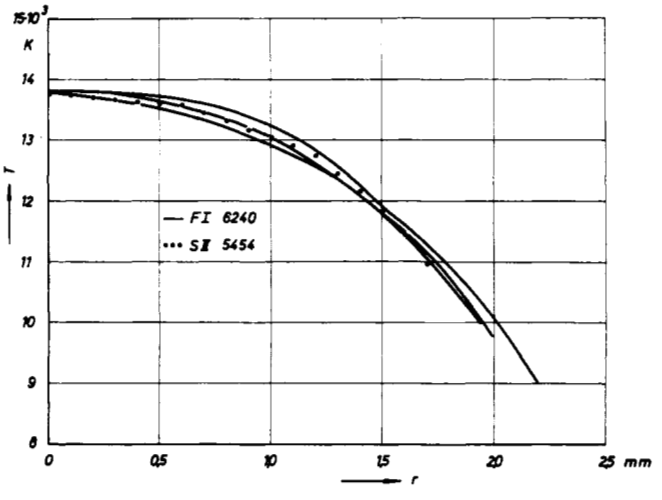

Fig. 7. Radial temperature distribution of a 100-A SF_6 arc (channel diameter 5 mm).

enthalpy h, electrical conductivity σ, and the thermal conductivity κ are particularly important properties of the arc. Their behavior, in the temperature range up to 30 000 K, is shown in Figs. 2–4. Some of these calculations can be readily checked experimentally using a stationary cylindrically symmetrical cascade arc [3], free of flow, burning at constant pressure. The system of basic equations, comprising Ohm's law, the radiation equation, and the power balance equation can be solved provided the current-field characteristic and, with certain restrictions, the current–radiation characteristic have been measured, and radiation densities and the electrical conductivity σ as a function of the heat flux potential S as well as the radial distribution of S have been obtained in this way [4]. Calorimetric measurements [5] give a more accurate value of E for SF_6 arcs than the method of steady-state auxiliary currents described by Maecker [6]. The $E(I)$ characteristics measured in the cascade arc in SF_6 and other gases are shown in Fig. 5. Over the range covered by the measurements, referring to equal currents, only the power in A is below that in SF_6. (The argon characteristic is not drawn in Fig. 5). In Fig. 6 the corresponding radiation characteristics are presented, the power dissipated in radiation being converted into equivalent values of E. The determination of the temperature distribution from measurements of absolute spectral line intensities in the arc makes it possible to relate temperature values to the radial distribution of S and hence to obtain the electrical conductivity $\sigma(T)$. As an example, Fig. 7 gives the temperature distribution in a 100-A SF_6 arc. The thermal conductivity $\kappa(T)$ is derived by differentiation of the equation

$$S = \int_{T_0}^{T} \kappa dT$$

which, in fact, defines S, and the excellent agreement between the measured and theoretical values of both functions is illustrated in Figs. 8 and 9 [7].

The temperature measurements also provide evidence for the demixing effects predicted by Frie's calculations [8]. Assuming local thermodynamic equilibrium, the intensities of spectral lines in the plasma can be determined as a function of temperature using the particle density diagram. In the absence of demixing, the intensity of the ionized sulphur line, shown in Fig. 7, and calculated up to 18 000 K, increases monotonically over the whole region whereas, when demixing effects are considered, it begins to fall again at temperatures below 14 000 K. Without demixing, the temperatures near the axis, determined from absolute intensity measurements, would be considerably lower than those obtained from measurements of the fluorine line and the monotonic increase toward the axis would no longer be observed [9]. Reference to Fig. 10, which shows the measured radial intensity distributions, clarifies the situation. The maximum is not in the axis. The experimental value of $7.14 \times 10^4\ W \cdot m^{-3} \cdot sr^{-1}$ agrees very well with the theoretical value, $8 \times 10^4\ W \cdot m^{-3} \cdot sr^{-1}$, calculated using the most recent value of the transition probability, when it is considered that the background pressure, 5 percent below normal, was not taken into account in the experiments and that the intensity, as indicated by calculations carried out

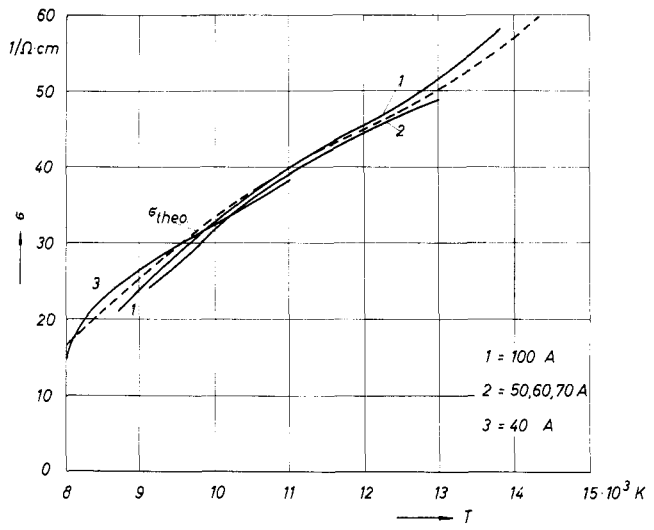

Fig. 8. Electrical conductivity of SF_6, experimental and theoretical values.

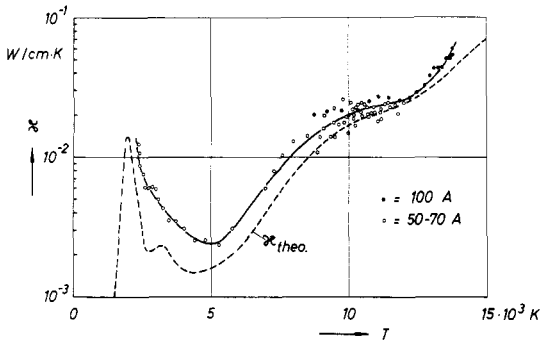

Fig. 9. Thermal conductivity of SF_6, experimental and theoretical values.

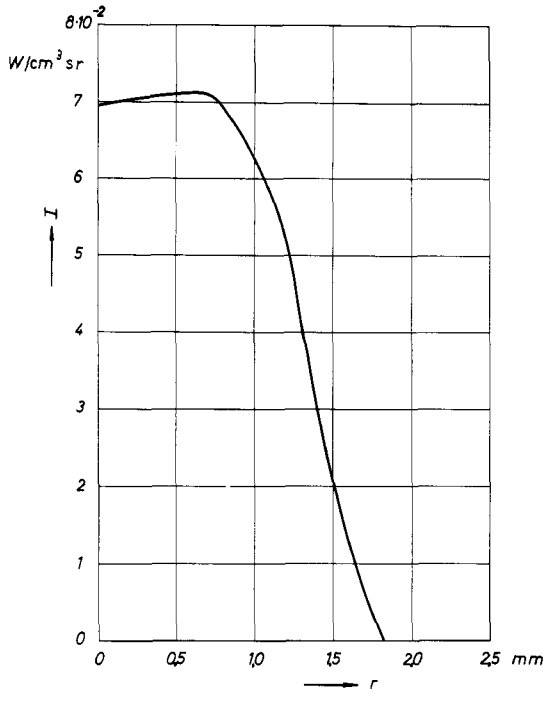

Fig. 10. Measured radial intensity distribution of the sulphur-ion spectral line 545.4 nm in a 100-A SF_6 arc.

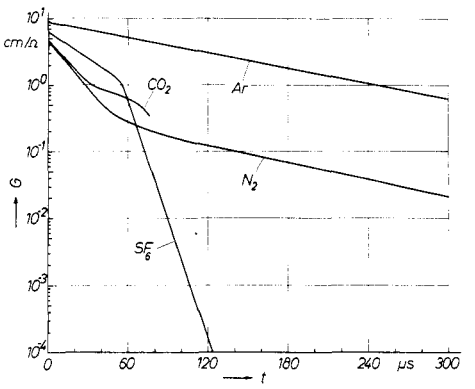

Fig. 11. Temporal decay of the conductance in interrupted cascade arcs.

at different pressures, is more than a linear function of pressure. Over the measured range, the demixing effect altered the particle density by as much as a factor of four.

III. Measurements on Nonsteady-State Arcs

The present state of art of circuit breaker arcs and, more generally, of the quenching process, is relatively poor. The latter process represents an extremely complicated problem in plasma physics and in view of the fact that simultaneous thermal, gas-dynamical, and electromagnetic processes occur the lack of understanding is not surprising. The rapidly changing turbulent and usually asymmetrical circuit breaker arc plasma is not suitable for certain physical measurements. To gain an insight into the dynamic plasma properties it is necessary to separate the various processes and study them under simpler conditions.

One important property of a plasma, the thermal conductivity and its influence on arc cooling, has been estimated by measuring the conductance of interrupted cascade arcs. A cascade arc, similar to that described by Maecker, was used in which the channel diameter was 5 mm and the arrangement was designed to have low inductance. The 100-A dc arc, burning at atmospheric pressure, was interrupted by means of a shorting spark gap connected in parallel with it. At a predetermined time after arc interruption, current steps were fed into the decaying cylindrically symmetric column. The current, and the resulting voltage drop across the column, were recorded on an oscilloscope. The time dependence of the electrical conductance after arc interruption was determined by varying the moment of step application since the interruption process was accurately reproducible. Conductance curves for A, N_2, CO_2, and SF_6 are shown in Fig. 11. Obviously, the different phases are related to the decay time constants shown in Fig. 12. It is clearly seen that, in contrast to the decay of the molecular gas which is associated with at least two time constants, the decay in the monatomic gas, argon, can be described by only one time constant during the first 400 μs after interruption. The steep decay in the conductance in SF_6 after 40–50 μs should be noted since this indicates a particulary efficient cooling by the heat conduction processes. It cannot be caused by electron attachment because the arc temperature is still too high for

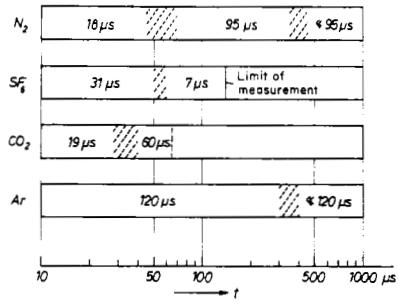

Fig. 12. Experimental time constants for the conductance decay in several gases.

TABLE I
CALCULATED CHANNEL PARAMETERS AND TIME CONSTANTS FOR THE INITIAL CONDUCTANCE DECAY

	r_k (cm)	σ_k ($cm^{-1} \cdot \Omega^{-1}$)	T_k (°K)	θ_G (μs)	θ_{exp} (μs)
N_2	0.17	50	12 000	23.3	18
SF_6	0.213	43.6	11 800	33.7	31
CO_2	0.172	50	12 400	15.7	19
Ar	0.227	53	12 250	132	120

Note: r_k, channel radius; σ_k, electrical conductivity; T_k, channel temperature; θ_G, calculated time constants; θ_{exp}, experimental time constants.

efficient attachment processes to take place. A formula for the decay time constants immediately following interruption can be derived by means of a channel model. The formula, which is given below, allows estimation of the time constants when the material data and the temperature profile of the stationary arc are known [10]. The formula is

$$\theta = \frac{1}{T_0}\left(\frac{dT}{d\sigma}\right)_{T_k} \cdot (\rho \cdot h)_{T_k} \cdot \frac{G}{N_0}.$$

The meanings of the symbols are as follows:

θ Time constant of conductance decay.
T Absolute temperature.
$\sigma(T)$ Electrical conductivity.
$h(T)$ Specific enthalpy.
T_0 A normalization temperature to be taken from the enthalpy curve.
ρ Density.
$G = \pi r_k^2 \sigma_k$ Electrical conductance per unit length.
r_k Channel radius.
σ_k Channel conductivity.
T_k Channel temperature.
} These quantities can be derived from the $\sigma(r)$ distribution [10].
N_0 Power input to the steady-state arc per unit length.

The initial time constants calculated using the formula previously mentioned, together with the experimentally determined values, are given in Table I.

The complete conductance curves can be explained by taking into account the relaxation processes and especially the transport of reaction energy when considering the heat dissipation [11]. This will be reported in detail elsewhere in the near future.

Another process, apart from transport phenomena such as heat conduction and radiation, which is of considerable importance in circuit breaker technology is the gas flow. The experimental arrangement used to make spectroscopic measurements of temperature in a gas blast arc is briefly described in the following. The arc burned through a 3-mm diameter conically shaped nozzle in front of which the quenching gas was introduced (see Fig. 13). The gas flow was in the axial direction. Steady burning was facilitated by immersing the tungsten pin cathode in an inert gas atmosphere. The annular anode, mounted downstream outside the burning chamber, was 3 cm from the cathode. The power input to the arc could be interrupted in less than 1.5 μs by means of a thyristor controlled short-circuiting connection. Measurement of the temperature profiles of the arc before and after interruption enabled a more complete understanding of the influence of gas flow cooling on the plasma decay to be obtained. The temperature was determined through its known dependence on the absolute intensity of the spectral lines which was the experimentally measured parameter.

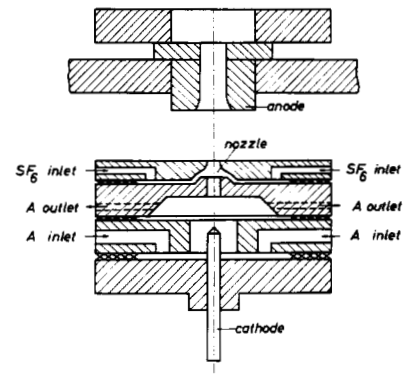

Fig. 13. Experimental device for 200-A dc arc with strong gas flow.

The arc was observed directly at the nozzle exit. The optical image of its longitudinal axis was arranged to be parallel to the entrance slit of the spectrograph and the arc length was limited to 0.6 mm by means of a diaphragm. The arc itself could be shifted perpendicular to the optical axis (x direction) and hence different regions of the arc cross section could be observed. A photomultiplier was used to register the line intensity. Interrupting the arc at different positions x yielded the intensity $I = I(t, x)$ and so enabled the intensity profiles $I(x)$ at different times after arc interruption to be deduced. Using the well-known transformation into radial intensity, the $I(r)$ profile and subsequently the $T(r)$ profile was derived. From the family of $T(r)$ profiles for a 200-A SF_6 arc at different times shown in Fig. 14 it is obvious that the decay process is caused not only by the decline of the temperature on the axis but also by the decrease in the arc radius. (The pressure in SF_6 was 2.5×10^5 N/m^2, in N_2 3.5×10^5 N/m^2. The mass flow rate in the two gases was 6 g/s. In the narrowest cross section the gas was flowing with sound velocity.)

The previously discussed temperature profile can be converted into electrical conductivity profiles using the material function $\sigma(T)$ shown in Fig. 3. Integration of the

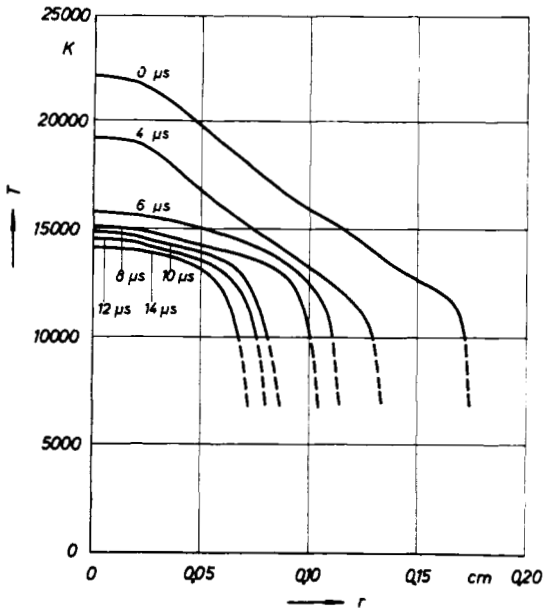

Fig. 14. Temperature profiles $T(r)$ of a gas blown interrupted SF_6 arc (200 A).

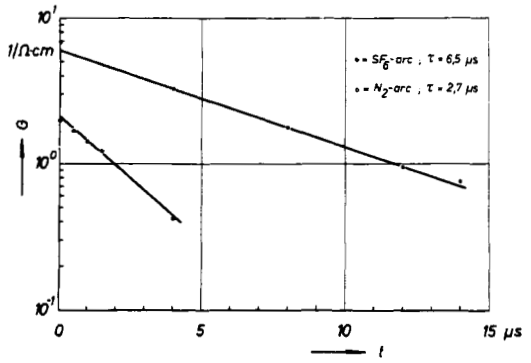

Fig. 15. Decay of the electrical conductance in a gas blown arc after interruption.

expression

$$G = 2\pi \int_0^R \sigma(r)\, r dr$$

gives the electrical conductance G per cm arc length. The electric field E follows from $E = i/G$ provided the current i is known. $E = 33$ V/cm is found for the steady-state arc ($t = 0$) in agreement with electrical measurements inside the nozzle.

Fig. 15 is obtained by plotting logarithmically the conductance G found in this way from the $T(r, t)$ profiles against time for the first 15 μs. This yields straight lines for both SF_6 and N_2 arcs, which were studied for comparison, corresponding to time constants, τ, of 6.5 μs and 2.7 μs, respectively.

According to Frind [12], the conductance time constant of a decaying arc is given by $\theta = r_0^2/(2.4^2 \times k)$, r_0 being the arc radius and $k = \kappa/\rho c_p$ the thermal diffusivity. Taking $r = 1.6$ mm from the temperature and $k = 0.05$ m^2/s for a medium temperature $T = 16\,000$ K, obtained by taking the average over the $T(r)$ profile, yields $\theta = 9$ μs which agrees fairly closely with the measured value. In the case of N_2, due

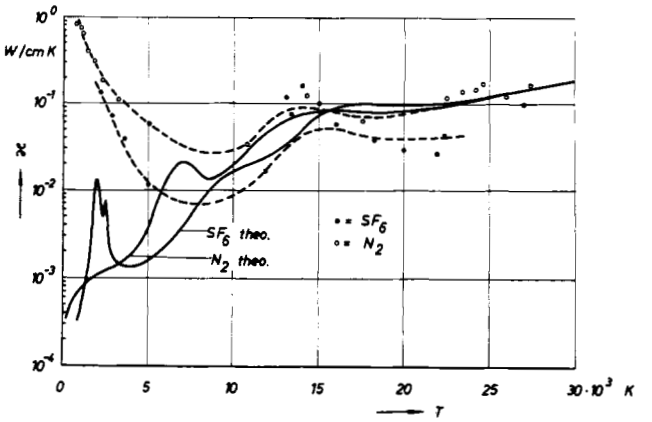

Fig. 16. Thermal conductivities evaluated from the temperature profiles of Fig. 14.

to the fact that the interruption time of 1.5 μs is not small compared with the decay time, the theoretical value is found to be lower than that determined experimentally. Comparison of the time constants given in Fig. 12 with those in Fig. 15 shows that the temperature measurements reflect only the initial behavior for the conductance decay. With the present apparatus, temperatures below about 10 000 K and the maximum axis temperature of about 23 000 K cannot be measured simultaneously because of the excessive differences in spectral line intensities.

The lower time constants of a blast arc compared to an arc without blast can be explained, in accordance with the previous considerations, in terms of the reduced arc radius. In both cases, Figs. 11 and 15, the initial time constant is smaller for N_2 than for SF_6, which means that the good quenching properties of SF_6 result from processes occurring in the temperature region below 10 000 K. In addition, the thermal conductivity coefficients κ can also be determined as a function of temperature from the steady-state temperature profiles by using the energy balance equation in its simplest form; i.e., only considering radial heat conduction and neglecting radiation and convection. The equation, in cylindrical coordinates, is

$$-\frac{1}{r}\frac{d}{dr}\left(r\kappa\frac{dT}{dr}\right) = \sigma E^2$$

or in more convenient form for the present calculation

$$\kappa(r) = -\frac{E^2}{r\left(\frac{dT}{dr}\right)_r}\int_0^r \sigma(r) r dr.$$

Hence κ can be determined by graphical integration of $r\sigma(r)$ and graphical differentiation of $T(r)$. The result of these calculations is shown in Fig. 16. For N_2 and SF_6 arcs in the temperature range 11 000–27 000 K, the values obtained in this way agree, within the expected error limits, with Frie's theoretical data, deviations of a factor of 2 for SF_6 being within the experimental error. Below 11 000 K the experimental values are larger than those predicted theoretically as a result of the steep temperature gradient. Although the assumption that heat is dissipated solely by

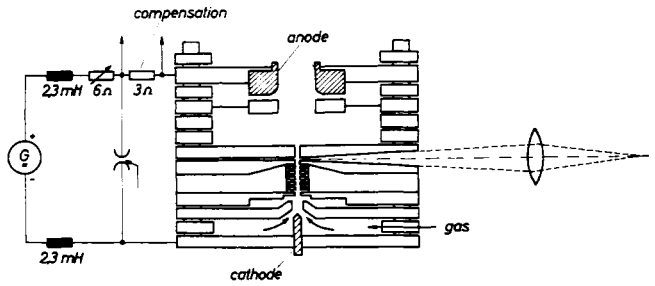

Fig. 17. Experimental setup for investigations of blown interrupted dc arcs.

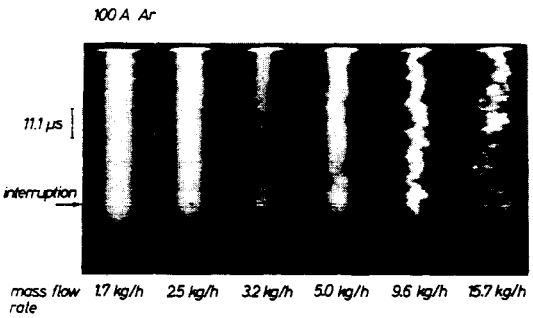

Fig. 18. Image converter streak photographs of interrupted blown argon arcs.

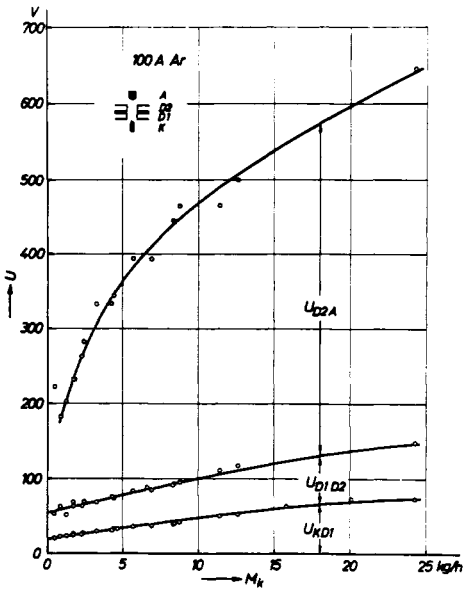

Fig. 19. Voltage distribution of a blow argon arc as function of the mass flow rate.

radial conduction in the inner regions of the arc seems justified by the agreement between the theoretical and experimental data, heat dissipation in the outer arc layers is increased by turbulence leading to large values of κ. Consequently, a very steep temperature profile is imposed on an arc burning through a nozzle by the relatively cool turbulent external layers. In contrast to the situation in the outer layers, the flow in the electrically conducting regions is laminar and the dominant heat dissipation process is radial heat conduction. The heat is then conducted away by the turbulent flow layers in the outer arc. The strong dependence of this type of investigation on the chosen geometry is shown in the following figures which refer to an interrupted dc gas blast arc burning in a cascaded cylindrical channel 5 mm in diameter and 20 mm long (see Fig. 17).

The gas inlet was in the cathode region where a high pressure buffer volume was formed and the gas streamed into free atmosphere through the channel. The annular anode was fixed approximately 2 cm above the channel. The luminosity distribution over a cross section of the arc perpendicular to the axis was photographed close to the channel exit using an image converter streak camera. The streak pictures of argon arcs given in Fig. 18 show clearly the initial decrease in the arc diameter as the mass flow rate was increased. The duration of luminosity after current interruption is seen to decrease in a similar manner. Instability of the arc column which set in at a mass flow rate of 5 kg/h, became more pronounced as the gas flow was increased until the arc wandering eventually covered the entire cross section of the channel. Measurements of the voltage across the channel showed a steady transition from stable to unstable burning (cf., Fig. 19). N_2 and SF_6 arcs were found to exhibit similar behavior.

IV. Investigations of Arcs Similar to those in Circuit Breakers

Ac arc investigations were carried out using the circuit-breaker-like twin nozzle arrangement shown schematically in Fig. 20. A 1000-A ac arc burned between the tubular electrodes (5 mm ϕ). The quenching agent SF_6 flowed axially from the upstream distributor rings towards the chamber centre where, after turning inward, it formed a radial blast into the arc before streaming through the tubular electrodes to the low pressure exit sections. The inter-electrode region was photographed with a high speed framing light fibre camera [13]. Fig. 21 shows a sequence of frames (5×10^5 frames/s) taken near current maximum. The bright plasma core protruding from the left-hand electrode is a metal vapor jet. (The vertical structure of the frames is caused by the light fibre band technique). The possibility that metal vapor may enter the inter-electrode gap against the gas flow in such arrangements is proved in Fig. 22 in which a twin-trace rotating drum camera exposure of a cross section perpendicular to the arc axis between the electrodes is portrayed. The upper trace was taken in integrated light and the lower trace was exposed simultaneously to the light of a copper spectral line (515.3 nm) using a monochromator. The periodic bursts seen in the integral light are clearly identifiable as metal vapor. Since the presence of metal vapor has a strong influence on electrical conductivity it is necessary to investigate more closely its effect on quenching and dielectric reignition. The spectra shown in Fig. 23 prove that metal vapor in the electrode gap can be avoided by using sufficiently large flowoff cross sections. The exposures were obtained during the falling part of the current half wave using a double nozzle model switch with arc catchers. The diameter of the nozzles was 10.4 mm. The approximately equal lengths of the F I and S II lines indicate a very steep temperature gradient in the outer arc regions which was measured

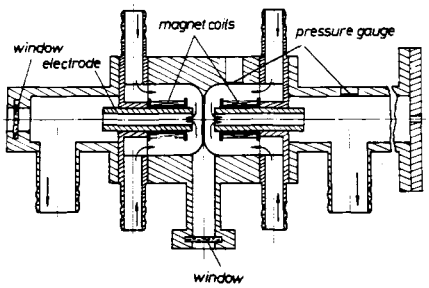

Fig. 20. Double nozzle arc chamber.

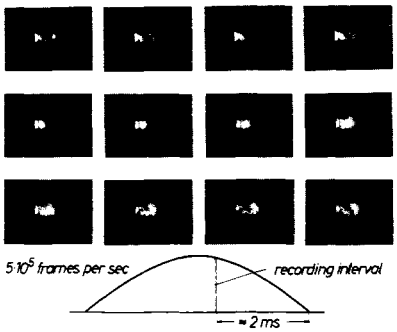

Fig. 21. Framing picture series of an ac discharge (100 Hz) with superimposed SF_6 gas flow (the arrows indicate the direction of gas flow).

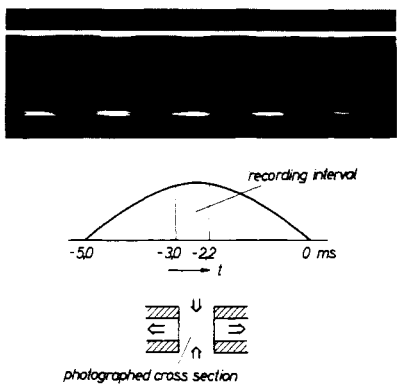

Fig. 22. Double trace streak photograph of an ac discharge with superimposed SF_6 gas flow. Upper trace, integrated light from the discharge; lower trace, light from the copper spectral line 515.3 nm.

to be about 2×10^5 K/cm. There are no metal lines in these spectra. The arc diameter taken from the luminous trace of a neutral line of fluorine was about 9 mm for an effective arc current of 4.7 kA. At the arc centre, temperatures of about 25 000 K, at which spectral lines of fluorine ions were observed, were attained. The temperatures at the visible arc edge were approximately 10 000 K. The increasing radius of luminosity and the nearly unchanged ratio of spectral lines of certain ionization states in the spectra indicate that there are only comparatively small variations in the central temperatures. The arc accommodates itself to the falling current by a decrease in its cross section rather than by a change in its conductivity since the temperature distribution and hence the conductance distribution in the arc are flat.

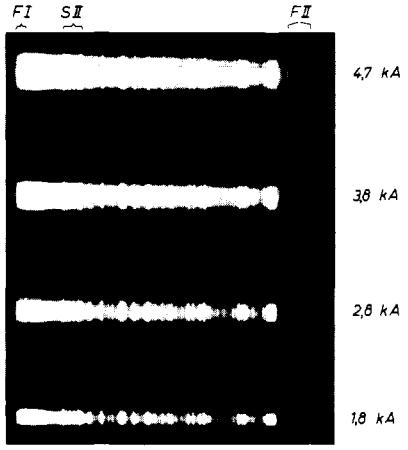

Fig. 23. SF_6 spectra from ac discharges (50 Hz) in a double nozzle model circuit breaker.

V. Conclusions

The measurements and observations described previously clearly illustrate the complicated nature of the physical processes occurring in gas-blast circuit breaker arcs. The sensitivity of the arc behavior to the experimental conditions (large changes in arc behavior for small changes in experimental conditions) is also in evidence. The results indicate that in order to understand the quenching process better, the problems of turbulent flow and transport as well as the electrode phenomena associated with it must be more fully investigated.

References

[1] R. E. Friedrich and R. N. Yeckley, "A new concept in power circuit-breaker design utilising SF_6," *AIEE Trans. Power App. Sys.*, vol. 68, Oct. 1959, pp. 695–706.

[2] W. Frie, "Berechnung der Gaszusammensetzung und der Materialfunktionen von SF_6," *Z. Phys.*, vol. 201, 1967, pp. 269–294.

[3] H. Maecker, "Ein zylindrischer Bogen für hohe Leistungen," *Z. Naturforsch. A.*, vol. 11, 1956, pp. 457–459.

[4] J. Uhlenbusch, "Berechnung der Materialfunktionen eines Stickstoff- und Argonplasmas aus gemessenen Bogendaten," *Z. Phys.*, vol. 179, 1964, pp. 347–366.

[5] H. Motschmann, "Über die experimentelle Bestimmung der Wärmeleitfähigkeit und der elektrischen Leitfähigkeit von Wasserstoff und Schwefelhexafluorid im elektrischen Lichtbogen," *Z. Phys.*, vol. 191, 1966, pp. 10–23.

[6] H. Maecker, "Messung und Auswertung von Bogencharakteristiken (Ar, N_2)," *Z. Phys.*, vol. 158, 1960, pp. 392–404.

[7] H. Motschmann, "Experimentelle Bestimmung der Wärmeleitfähigkeit und der elektrischen Leitfähigkeit von Schwefelhexafluorid im Temperaturbereich unterhalb 9 000 K," *Z. Phys.*, vol. 205, 1967, pp. 235–248.

[8] W. Frie, "Entmischungseffekte ionisierender Atomgase," *Z. Phys.*, vol. 214, 1963, pp. 42–56.

[9] H. Motschmann, "Prüfung der Plasmaentmischung und Bestimmung einiger Materialfunktionen von Schwefelhexafluorid mittels Temperaturmessung am 100-A-Kaskadenbogen," *Z. Phys.*, vol. 214, 1968, pp. 42–56.

[10] W. Hertz, "Determination of the conductance decay time constants of interrupted arcs by the aid of a channel model," *Proc. 9th Int. Conf. on Phenomena in Ionized Gases* (Bucharest, 1969), p. 296.

[11] ——, Ph.D. dissertation, Technical University of Munich, Munich, Germany, 1970.

[12] G. Frind, Über das Abklingen von Lichtbogen," *Z. Angew. Phys.*, vol. 12, 1960, pp. 231–237.

[13] W. Hertz, "Eine Mehrspurtrommelkamera mit Lichtleitbändern," *Optik*, vol. 29, 1969, pp. 491–497.

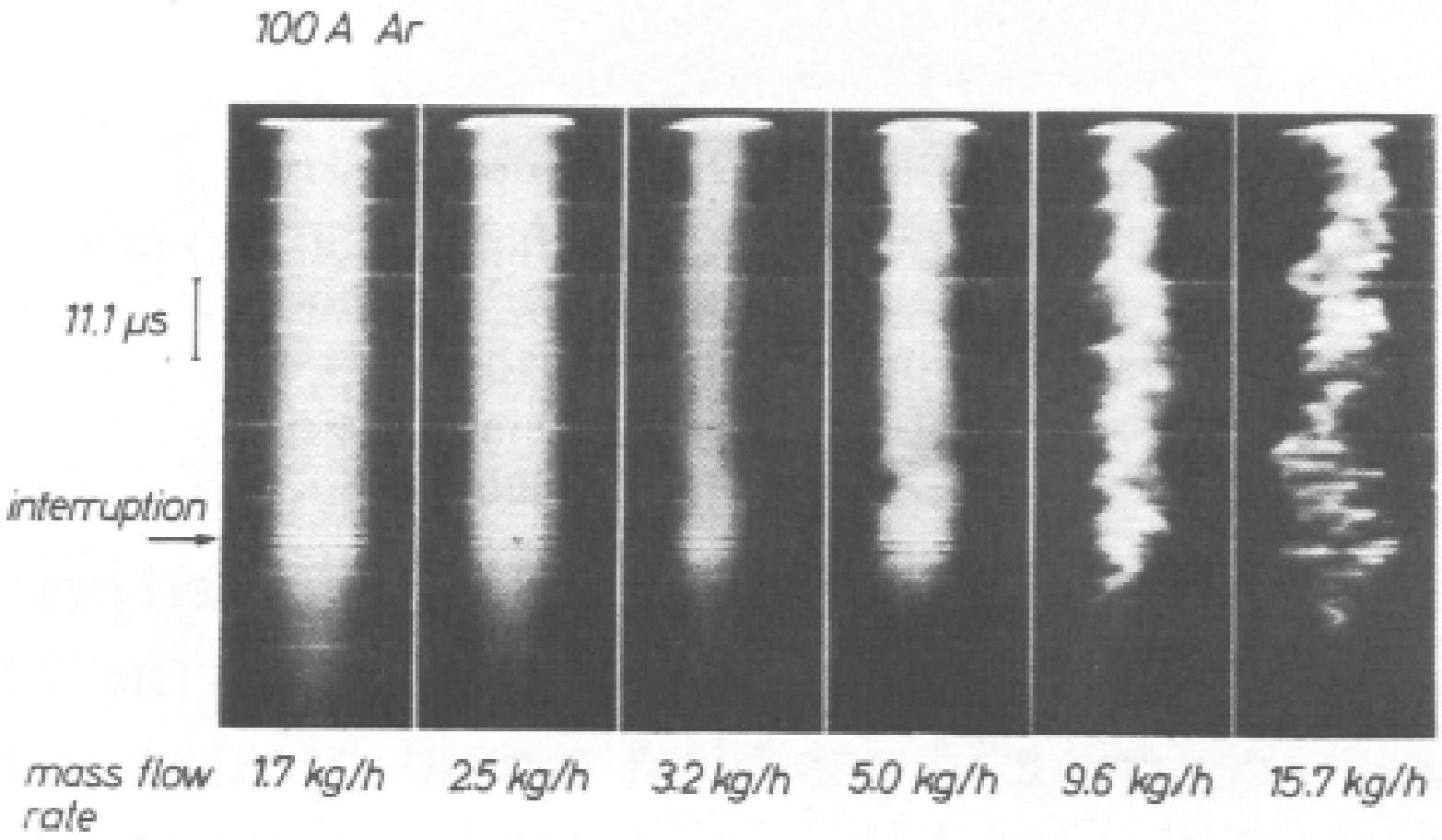

Fig. 18. Image converter streak photographs of interrupted blown argon arcs.

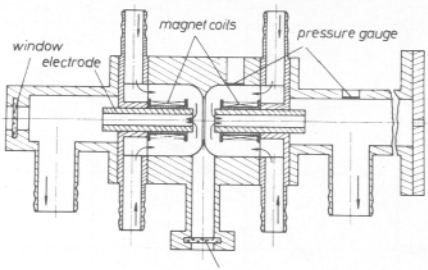

Fig. 20. Double nozzle arc chamber.

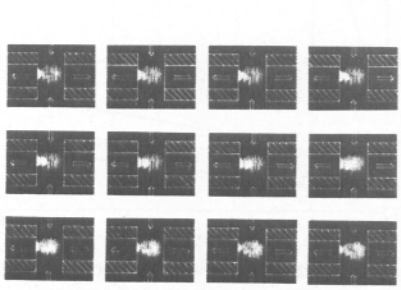

Fig. 21. Framing picture series of an ac discharge (100 Hz) with superimposed SF_6 gas flow (the arrows indicate the direction of gas flow).

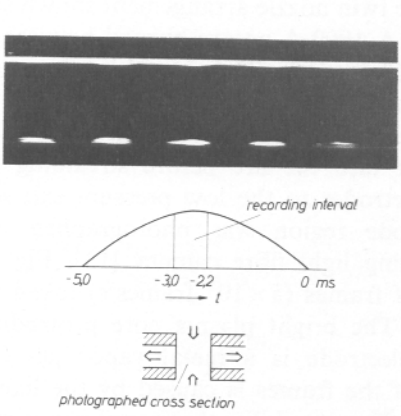

Fig. 22. Double trace streak photograph of an ac discharge with superimposed SF_6 gas flow. Upper trace, integrated light from the discharge; lower trace, light from the copper spectral line 515.3 nm.

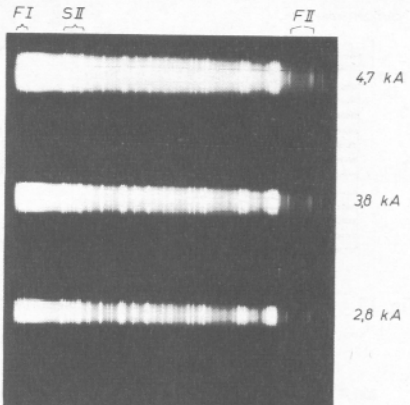

Fig. 23. SF_6 spectra from ac discharges (50 Hz) in a double nozzle model circuit breaker.

V. Conclusions

The measurements and observations described previ clearly illustrate the complicated nature of the phy processes occurring in gas-blast circuit breaker arcs. sensitivity of the arc behavior to the experimental co tions (large changes in arc behavior for small chang experimental conditions) is also in evidence. The result dicate that in order to understand the quenching pro better, the problems of turbulent flow and transport as as the electrode phenomena associated with it must be m fully investigated.

References

[1] R. E. Friedrich and R. N. Yeckley, "A new concept in power ci breaker design utilising SF_6," *AIEE Trans. Power App. Sys.*, vo Oct. 1959, pp. 695–706.

[2] W. Frie, "Berechnung der Gaszusammensetzung und der Ma funktionen von SF_6," *Z. Phys.*, vol. 201, 1967, pp. 269–294.

[3] H. Maecker, "Ein zylindrischer Bogen für hohe Leistungen *Naturforsch. A.*, vol. 11, 1956, pp. 457–459.

[4] J. Uhlenbusch, "Berechnung der Materialfunktionen eines stoff- und Argonplasmas aus gemessenen Bogendaten," *Z.* vol. 179, 1964, pp. 347–366.

[5] H. Motschmann, "Über die experimentelle Bestimmung der meleitfähigkeit und der elektrischen Leitfähigkeit von Wasse und Schwefelhexafluorid im elektrischen Lichtbogen," *Z. Phys.* 191, 1966, pp. 10–23.

[6] H. Maecker, "Messung und Auswertung von Bogencharg